JOURNAL OF GEOPHYSICAL RESEARCH, VOL. 109, C04024, doi:10.1029/2003JC001912, 2004

Shelfbreak circulation in the Alaskan Beaufort Sea: Mean structure and variability

Robert S. Pickart

Department of Physical Oceanography, Woods Hole Oceanographic Institution, Woods Hole, Massachusetts, USA

Received 14 April 2003; revised 6 January 2004; accepted 9 March 2004; published 24 April 2004.

[1] Historical hydrographic and current meter data are used to investigate the properties and circulation at the shelf edge of the Alaskan Beaufort Sea. Thirty-three individual cross-sections, spanning the time period 1950 to 1987, are combined in a topographical framework to produce mean vertical hydrographic sections, as well as a section of mean absolute geostrophic velocity referenced using the current meter data. This reveals the presence of a narrow (order 20 km) eastward current, referred to as the Beaufort shelfbreak jet. The jet has three distinct seasonal configurations: In late-spring to late-summer, cold, winter-transformed Bering water is advected in a subsurface current; from mid-summer to early fall a surface intensified current advects predominantly Bering summer water; and from mid-fall to mid-spring, under easterly winds, the jet transports upwelled Atlantic water. The volume transport of the jet represents a significant fraction of the inflowing transport through Bering Strait. While the characteristics and flow of the winter-transformed Bering water vary interannually, this water mass ventilates predominantly the upper halocline. *INDEX TERMS:* 4512 Oceanography: Physical: Currents; 4528 Oceanography: Physical: Fronts and jets; 4536 Oceanography: Physical: Hydrography; *KEYWORDS:* boundary current, shelfbreak processes

Citation: Pickart, R. S. (2004), Shelfbreak circulation in the Alaskan Beaufort Sea: Mean structure and variability, *J. Geophys. Res.*, *109*, C04024, doi:10.1029/2003JC001912.

1. Introduction

[2] It is generally believed that the cold halocline of the Arctic Ocean is maintained by input of shelf-derived waters [*Aagaard et al.*, 1981]. However, the precise mechanisms by which this occurs are not well understood. In the western Arctic, the inflowing Pacific water clearly plays a fundamental role in the ventilation process, as some of this water ultimately feeds the interior of the Canada Basin. The question is, where and how does this injection occur? To help answer this, we need to understand how the Pacific water initially adjusts upon reaching the edge of the shelf.

[3] Pacific water enters the Arctic through Bering Strait. The mean transport of the inflow is 0.8 Sv [*Roach et al.*, 1995], though there is large variability on timescales from days to years. In summertime, most of the inflowing water continues northward in the Chukchi Sea as a coastal jet adjacent to Alaska: the Alaskan Coastal Current (Figure 1). Three distinct water masses are transported northward by this current (proceeding from light to dense): Alaskan Coastal water, Bering Seawater, and a third un-named water mass which is a mixture of Bering Shelf and Anadyr water [*Mountain*, 1974]. The first two are easily identified downstream by their anomalously warm summertime temperatures (as warm as 5°C), and sometimes they are considered as a single water mass [e.g., *Munchow and Carmack*, 1997; *Shimada et al.*, 2001]. In the present study, we refer to this composite water mass as summertime Bering water.

[4] During wintertime the resident waters of the Chukchi and Bering Seas are strongly modified by air-sea interaction and ice formation. The winds intensify from the northeast, weakening the flow through Bering Strait [*Weingartner et al.*, 1998], and the ice edge advances from north to south. In the northern Bering Sea, cold, brine-enriched water enters Bering Strait from the Gulf of Anadyr [*Muench et al.*, 1988], which is subject to further modification in the Chukchi Sea [*Weingartner et al.*, 1998]. Consequently, several distinct winter waters can be found north of Bering Strait (progressing from light to dense): Bering Sea winter water, Intermediate salinity water, and Hypersaline water [*Weingartner et al.*, 1998]. The latter seems to be mostly the product of coastal polynyas that tend to form northeast of Cape Lisburne [*Cavalieri and Martin*, 1994; *Weingartner et al.*, 1998; *Winsor and Chapman*, 2002]. Here we consider the first two as a single water mass called winter-transformed Bering water.

[5] During the period of winter modification and enhanced northeasterlies, the Alaskan Coastal Current can weaken considerably, and even partially reverse [*Weingartner et al.*, 1998]. During such periods the bulk of the inflowing water through Bering Strait (which itself is reduced) is diverted northwestward toward Herald Canyon [*Weingartner et al.*, 1998] (Figure 1). Hence the seasonal contrast of Pacific-origin water flowing through the Chukchi Sea toward the

0148-0227/04/2003JC001912$09.00

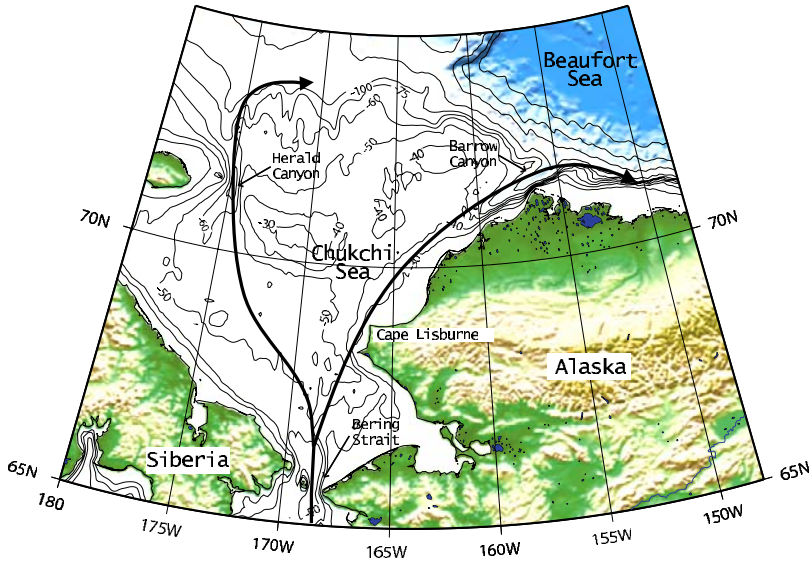

Figure 1. Schematic of the two main branches of Pacific-origin water flowing through the Chukchi Sea; the eastern branch is the Alaskan coastal current. Presumably, both branches turn and flow eastward toward the Beaufort Sea upon reaching the shelfbreak.

open Arctic is pronounced: In summer/fall a swift jet transports buoyant water, whereas in winter a weaker current, partitioned between different branches, advects dense water resulting from cooling and ice formation. After the winter winds relax, the dense water likely gets flushed out of the Chukchi Sea more rapidly. (Coincident with this, dense, salty water from the northern Bering Sea, originating from a polynya south of St. Lawrence Island, flows through Bering Strait [*Muench et al.*, 1988].)

[6] What happens to the water when it reaches the shelfbreak of the Canada Basin (Figure 1)? This is a matter of some uncertainty and debate. Early work suggests that during late summer to early fall, most of the eastern branch simply "turns the corner," skirting Barrow Canyon, as a coherent jet [*Mountain*, 1974; *Paquette and Bourke*, 1974]. This can be thought of as the extension of the Alaskan Coastal Current. This view is based on geostrophic calculations (referenced to a deep depth) and property distributions [*Mountain*, 1974; *Paquette and Bourke*, 1974]. More recent current meter data, however, are inconclusive as to what extent this is true (T. J. Weingartner, personal communication, 2002). *Aagaard* [1984] argued that a strong summertime frontal jet does not exist east of Point Barrow, although *Mountain* [1974] used some of the same data to arrive at the opposite conclusion. In late winter to early summer the situation is even less certain. The traditional view is that after the winter winds relax, much of the dense water from the eastern Chukchi Sea flows down Barrow Canyon and directly enters the interior Canada Basin [*Garrison and Becker*, 1976; *Weingartner et al.*, 1998]. However, dynamical constraints, supported by recent model results [*Chapman*, 2000], suggest that a large fraction of the dense wintertime water approaching Barrow Canyon may not exit through the canyon, but instead might adjust to deeper isobaths and also turn eastward. This is consistent with *Gawarkiewicz*'s [2000] model in which dense water from the shelf can not efficiently penetrate beyond the shelfbreak.

[7] In this study we use historical hydrographic and current meter data to try and present a clearer, more systematic view of the flow of Pacific water after it encounters the edge of the continental shelf. We focus on the region immediately east of Barrow Canyon (partly to avoid local canyon effects). We refer to this flow as the Beaufort shelfbreak current, or jet. We begin with a description of the historical data and the methods used to standardize them. Then a mean representation of the current is constructed, including an average absolute geostrophic velocity section referenced using the mean current meter data. This is followed by an investigation of the seasonal variability. We demonstrate that there are three basic configurations of the Beaufort shelfbreak jet: a surface-intensified flow transporting summertime Bering water, a mid-depth jet carrying winter-transformed Bering water, and a third state, involving the underlying Atlantic water, which occurs during the winter upwelling period. Finally, we consider the interannual variability of the current and discuss the associated ramifications for the ventilation of the halocline.

2. Data and Methods

[8] One of the primary aims of this study is to construct a robust mean description of the eastward-flowing Pacific water shortly after it encounters the shelf edge, as a starting point for subsequent investigation of how this water may be fluxed offshore and contribute to the ventilation of the cold halocline in the western Arctic. We tried to obtain all the available historical data within the domain of interest, defined as the region of the Alaskan Beaufort shelf and slope between Barrow Canyon and Mackenzie Canyon (Figure 2). The source of hydrographic data is the National Oceanographic Data Center (NODC) World Ocean Atlas 1994.

[9] In constructing regional climatologies it is common to average the data within a specified set of bins, not necessarily keeping track of the synopticity of the measurements.

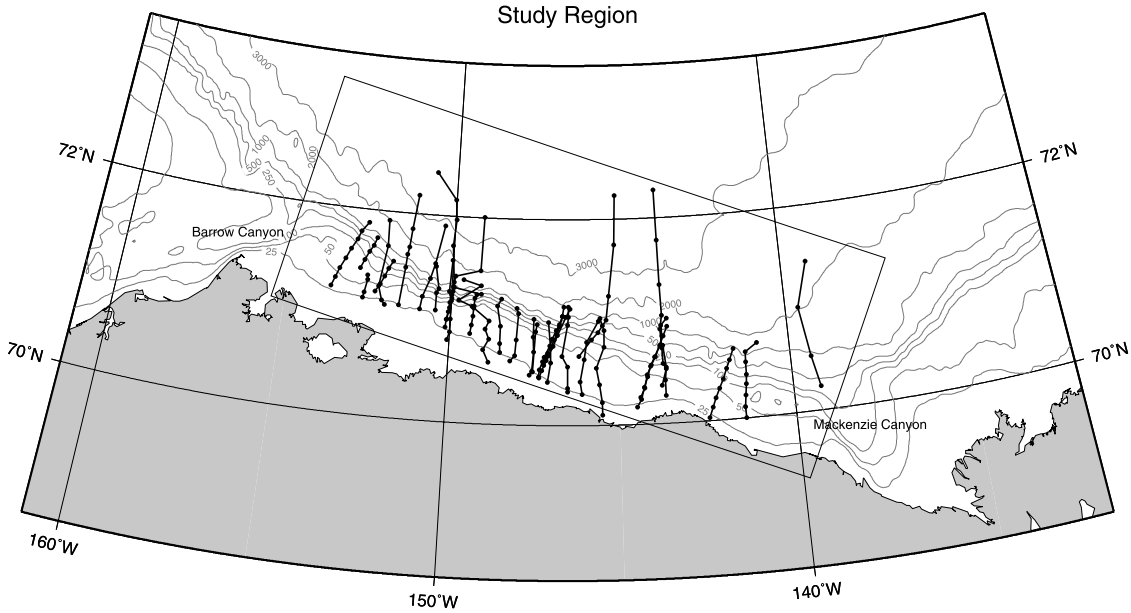

Figure 2. Historical hydrographic sections used in the analysis. The rectangle delimits the region used to compute the mean topography.

We tried such an approach here, but found that the relative sparseness of the data in the area of interest led to some spurious computed fields (this is elaborated on below). Hence we identified all the individual synoptic cross sections within the historical data set, then individually interpolated each one, to fill in cross-stream gaps, before any binning was done. This is similar to the approach that *Pickart* [1992] used to create an average section of the North Atlantic Deep Western Boundary Current.

2.1. Topography and Standard Grid

[10] The first step in the gridding process involved determining the bathymetry. We used the International Bathymetric Chart of the Arctic Ocean (IBCAO) digital database (2000 version). Since most of the NODC data in this region do not contain sonic depths, we used IBCAO to assign a bottom depth to each hydrographic cast according to its position. In some instances the deepest measurement depth, z_{max}, was greater than the corresponding IBCAO depth, in which case the bottom was (arbitrarily) set to be $z_{max} + 10$ m. (This occurred roughly 10% of the time.) Next, we computed an average cross-stream bottom depth profile as follows. The digital bathymetry, originally in a polar stereographic projection, was rotated and transformed into a Cartesian coordinate frame in which the mean orientation of the upper slope is aligned along the abscissa (Figure 3a). Then cross-stream slices were taken through the domain in order to compute an average bottom slope versus cross-stream distance curve. This in turn was integrated to obtain the average bottom profile shown in Figure 3b. The figure also shows the domain of our standard grid. Note that the shelfbreak occurs at roughly 50 m, although the bottom slope continues to steepen sharply offshore of this in the region of the upper slope.

[11] Following this step, the stations comprising each synoptic section were projected onto the standard grid by simply assigning station locations according to their bottom depth. We restricted our analysis to the upper 500 m because of the low data density deeper than this and because a large fraction of the data are bottle measurements which have a small signal-to-noise ratio in deep water. Potential temperature (θ) and potential density (σ_θ), referenced to the sea surface, were computed at each station and any density

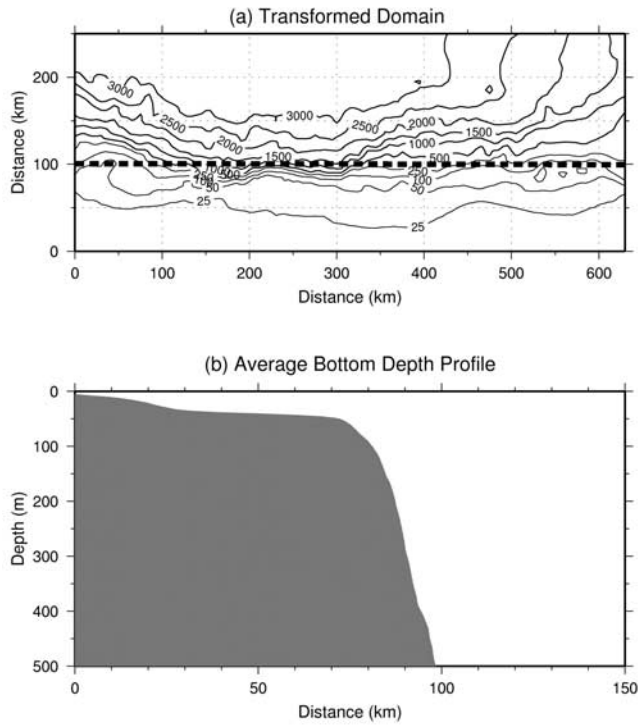

Figure 3. (a) The study domain after transforming into a Cartesian coordinate frame. The dashed line is the line of best fit to the 250-m isobath, used to define the orientation of the abscissa. (b) Domain of the standard grid and the mean cross-stream bottom profile.

inversions removed. Then Laplacian-Spline interpolation was used to interpolate the sections onto the uniform grid, with Δx = 5 km and Δz = 10 m.

[12] Several important aspects of this gridding process should be noted. Since our grid is finer than the average station spacing and bottle spacing, the objective interpolation "smartly" fills in areas between data points, which results in more uniform coverage for subsequent binning. Owing to the relatively small amount of data in the region, binning of the original data points alone (i.e., without prior interpolation) results in substantially noisier fields, particularly for the standard deviation fields. Note that our projection onto the standard grid is equivalent to aligning the sections in a topographic framework, which is sensible for a boundary current regime, with the added advantage of not doing the interpolation in bottom depth space (as was done, for instance, by *Linder and Gawarkiewicz* [1998] in their climatology of the middle Atlantic Bight). This is important in the vicinity of the shelfbreak, where the large change in depth is problematic for gridding in bottom depth space. Finally, having all the sections on the same grid allows for a more quantitative analysis, including the calculation of empirical orthogonal functions (see section 5).

2.2. Synoptic Sections

[13] Scrutiny of the NODC data set revealed 47 synoptic hydrographic sections within our domain. Unfortunately, nine of these sections were not contourable due to unacceptably large station spacing or minimal coverage in the vertical. Furthermore, some of the remaining sections were notably anomalous (though not necessarily containing bad data). To objectively identify such sections, which would skew the results, we applied the following simple procedure. One by one each section was omitted from the group, and the mean and standard deviation fields computed. Then the average standard deviation over the entire domain for each case was compared to that for the full collection of sections. This procedure revealed five particularly anomalous sections (four of them from a single cruise in 1985 which encountered abnormally warm conditions at depth) each of which increased the average standard deviation by more than 0.02°C. These sections were omitted, resulting in a total of 33 sections in our collection. While this may seem like a disappointingly small number, it should be remembered that this is a difficult area of the ocean to sample, and even a single well-resolved hydrographic section is hard to come by. As is clear by the results presented below, the final collection of sections produced robust, meaningful fields. The seasonal and yearly distribution of the sections is presented in Table 1. Note that all but four of the occupations were done in summer and fall.

[14] The reader should bear in mind that since the local bathymetry along each section differs from the average bottom profile of the standard grid, the relative station spacing of each section was altered in the gridding process. We computed the degree to which this occurred, and the histogram of the offsets (not shown) was sharply peaked within ±5 km, with a mean close to zero (1.5 km). Hence there was virtually no bias in the gridding process, and the majority of stations were not moved very far. Nonetheless there were significant offsets: The mean of the absolute value was slightly less than half the average station spacing.

Table 1. Historical Hydrographic Sections Used in the Study[a]

Section Number	Year	Month	Day	Approximate Longitude, °W
1	1950	8	27–28	145
2	1950	8	29–30	152
3	1951	9	14–21	140
4	1951	8	23–25	144
5	1951	8	28	151
6	1971	9	1–12	149
7	1971	9	10–13	150
8	1971	8	20–21	144
9	1971	8	22–23	146
10	1971	8	23–24	147
11	1971	8	29	147
12	1971	8	30–31	148
13	1972	9	3–5	152
14	1972	8	8–10	146
15	1972	8	11–14	147
16	1972	8	15	148
17	1972	8	17–20	149
18	1972	8	23–27	150
19	1975	11	6–10	142
20	1975	10	26–31	153
21	1976	11	1	149
22	1976	10	31	150
23	1976	11	3	152
24	1976	11	4	153
25	1976	5	23	147
26	1985	8	28–29	150
27	1986	10	13–14	141
28	1986	10	11–12	144
29	1986	10	8–9	147
30	1986	10	16–17	150
31	1987	4	11–14	144
32	1987	4	26–28	147
33	1987	4	18–21	153

[a]The subset of sections corresponding to the summer water case are 5, 11, 12, 13, 18, 28, 29; the winter water realizations are 1, 2, 6, 7, 9, 14, 15, 17, 33; the Atlantic water realizations are 19, 21, 23, 24, 31, 32.

This has the biggest impact on the thermal wind shear (which depends on station spacing), and consequently we did not compute the geostrophic velocity of the individual sections. However, the small bias and sharply peaked histogram leads to an accurate average thermal wind field. The distribution of hydrographic data in the cross-stream plane (Figure 4) shows that most of the data points are clustered around the shelfbreak. Fortunately, the number of realizations tapers off smoothly with distance and depth and hence does not create any artificial gradients due to data coverage.

3. Mean Fields

3.1. Hydrographic Properties

[15] One of the distinguishing features of the Arctic Ocean is the cold halocline, a subsurface layer of relatively uniform temperature and strong salinity gradients [see, e.g., *Aagaard et al.*, 1981]. This layer acts as a permanent shield between the ice cover and the warm Atlantic water at depth. Above the halocline the water column is well mixed in winter, while in summer a seasonal pycnocline can develop. To elucidate the structure of the halocline in this part of the Beaufort Sea, we computed the mean vertical profile of salinity (salinity is presented using the practical salinity scale and has no units) and its vertical derivative (Figure 5) at the seaward end of our mean hydrographic section (x = 130 km). One sees that the permanent halocline is roughly 100 m thick, centered near

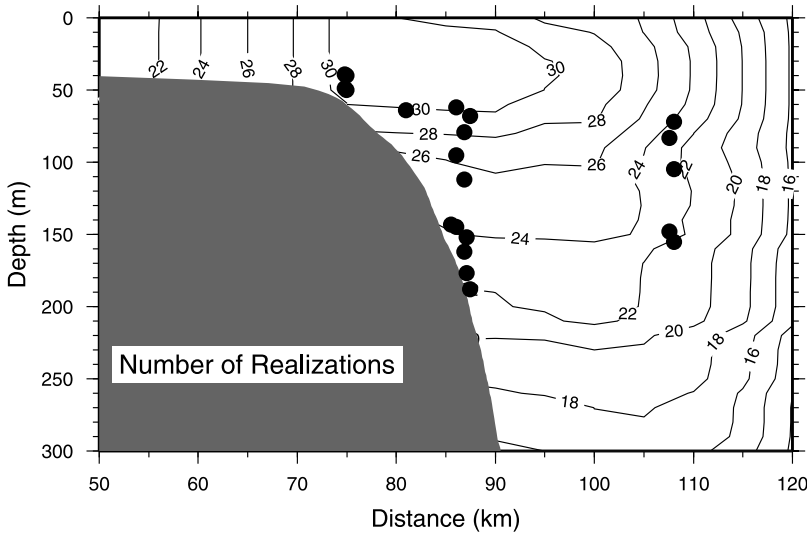

Figure 4. Number of realizations in the cross-stream plane (contours), and the positions of the mean current meter values (circles).

150 m. In the upper hundred meters a strong seasonal halocline is present, since our average is dominated by summer and fall sections (Table 1). Throughout the paper we will distinguish between the upper halocline (32.85–33.5) and the lower halocline (33.5–34.25). By way of comparison, *Melling* [1998] used individual salinity surfaces to represent the halocline in the Canadian Beaufort Sea: 33.1 (upper halocline), 33.5 (middle halocline), and 34.5 (lower halocline).

[16] The average hydrographic sections and associated standard deviation fields are presented in Figure 6. The potential temperature section shows the presence of a cold water mass adjacent to the upper slope: the winter-transformed Bering water. As mentioned earlier, this water is the most common winter product formed in the Chukchi Sea. It is high in silicate content because its source waters come from the Pacific and because of local regeneration of nutrients on the Chukchi shelf [*Jones and Anderson*, 1986]. It also contains an anomalous signature in transient tracers such as ^{210}Pb and the ^{228}Ra/^{226}Ra activity ratio [*Smith et al.*, 2003]. We were only able to obtain silicate data for four of the historical sections (from the fall of 1986), and used this information to construct an average vertical profile through the winter-transformed water (Figure 7). One sees the tight relationship between silicate and temperature (which was present in each of the individual sections as well), indicating that both quantities are an effective tracer of this water mass. Note in Figure 6a that the winter-transformed Bering water is ventilating primarily the upper halocline (the interannual variability of this water mass is discussed in section 5). This implies that the only water of Pacific origin that could ventilate the lower halocline of the southern Canada basin is the hypersaline dense water observed by *Weingartner et al.* [1998]. Since this

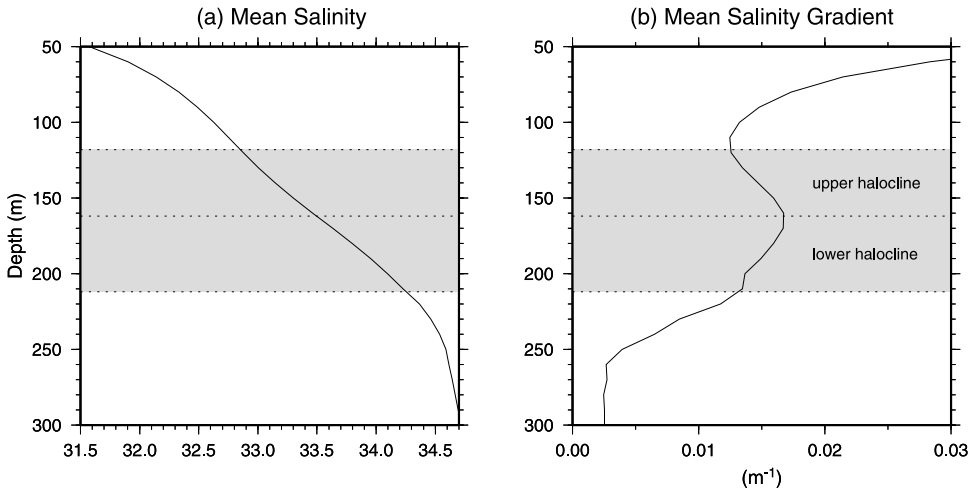

Figure 5. Mean vertical profiles at x = 130 km. (a) Salinity. (b) Vertical derivative of salinity. The shaded regions denote the upper and lower portions of the halocline.

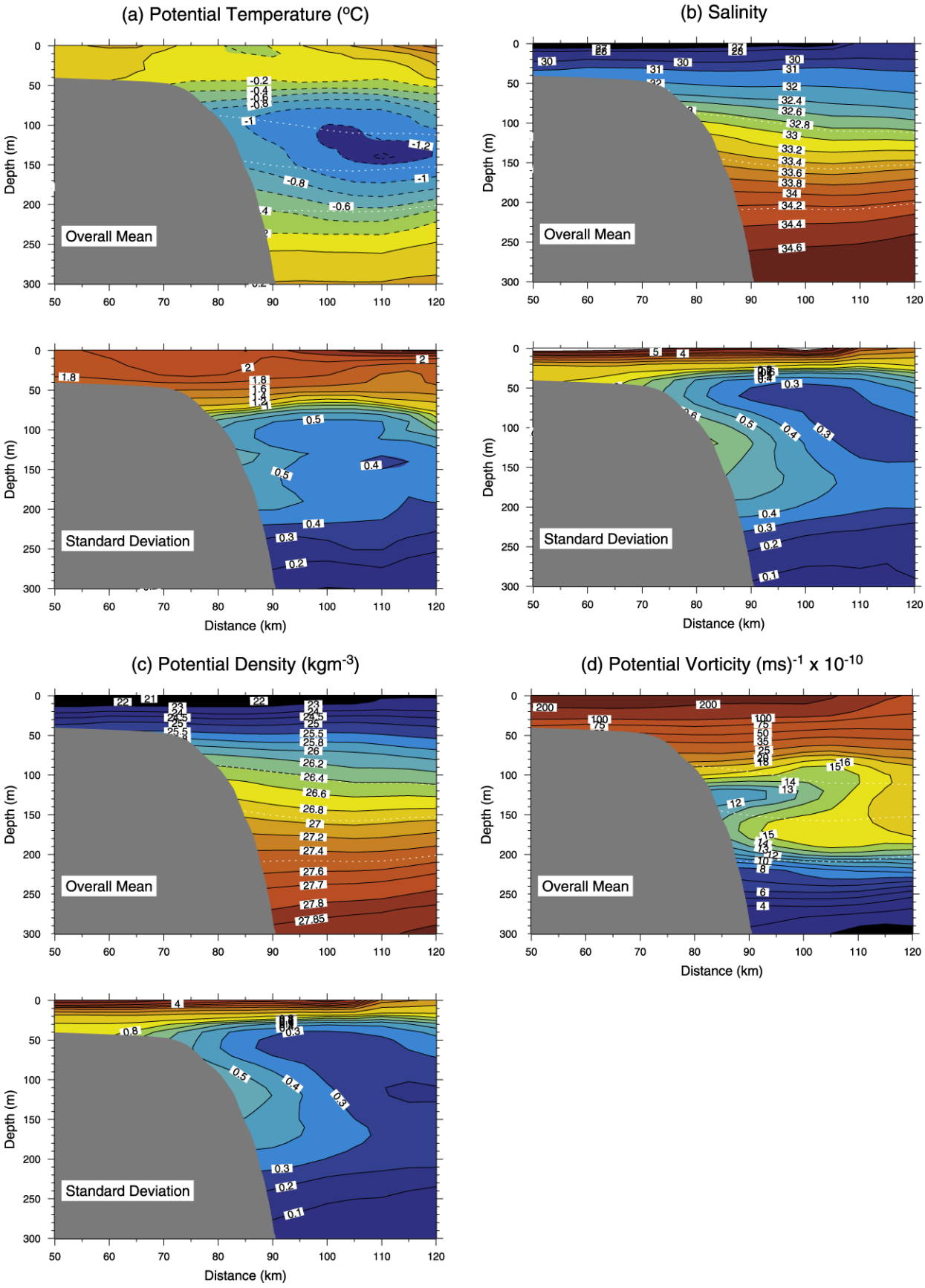

Figure 6. Mean hydrographic sections and standard deviations. The white dotted lines denote the upper and lower halocline as defined in Figure 5.

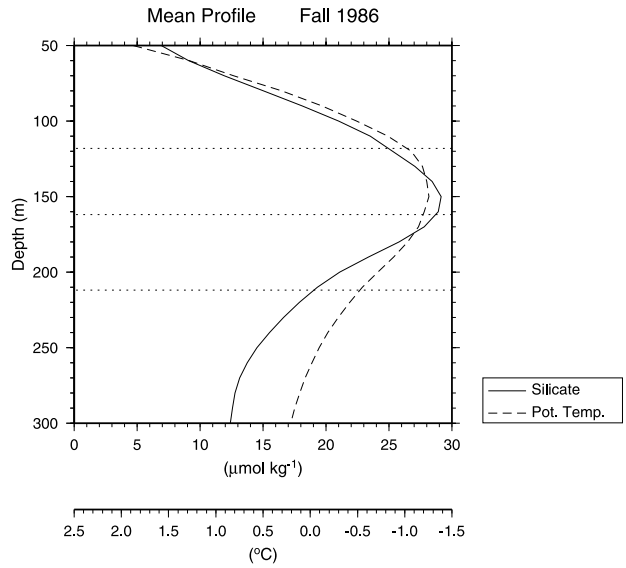

Figure 7. Average profiles of silicate (solid line) and potential temperature (dashed line) for the fall 1986 sections only. The average was computed over the lateral extent of the winter-transformed Bering water signal. The upper and lower portions of the halocline are indicated by the dotted lines.

dense water is likely formed only sporadically, it suggests that the lower halocline is predominantly renewed farther to the west along the Eurasian shelves.

[17] Winter-transformed Bering water is also found along the upper slope to the west of Barrow Canyon [*Weingartner et al.*, 1998], presumably having exited from Herald Canyon (Figure 1). Hence the cold temperature/high silicate core observed in our study region may be due to a combination of both of these outflows from the Chukchi shelf. Unlike the winter water, there is no obvious signature of the summertime Bering water in the mean temperature section. However, this water mass is present at the outer shelf and shelfbreak in some of the synoptic realizations (discussed below). Beneath the halocline, one sees the beginnings of the Atlantic water signature (temperatures greater than 0°C). This water mass is flowing eastward along the continental slope as part of a large-scale cyclonic boundary current system within the Arctic [e.g., *Rudels et al.*, 1994]. An expanded view of our mean section (not shown) indicates that at this location, the temperature maximum of the Atlantic water occurs at a depth of 450 m.

[18] The mean salinity and σ_θ sections (Figures 6b and 6c) show features similar to each other, since density is dominated by salinity at these cold temperatures. At the surface a fresh layer extends from the shelf some 30 km beyond the shelfbreak. The primary feature of interest in this study is the subsurface tilt of isopycnals adjacent to the upper slope. From about 75 m to 175 m the isopycnals slant upward toward the boundary (e.g., the 26.6 σ_θ contour), whereas deeper than this they slope downwards (e.g., the 27.7 σ_θ contour). Assuming that in the mean the flow in this portion of the water column is eastward, the associated thermal wind shear implies a subsurface jet with maximum velocity at the depth where the isopycnal tilt reverses. The spreading of isopycnals near the boundary results in a local pycnostad, which is seen clearly in the mean section of planetary potential vorticity, $(f/\rho)(\partial\rho/\partial z)$, where f = Coriolis parameter and ρ = density (Figure 6d). One sees the tongue of low potential vorticity extending from the boundary near 125 m. Note that this pycnostad weakens the signature of the upper halocline adjacent to the continental slope.

[19] The standard deviation fields reveal that the maximum variability occurs in the near-surface layer, associated with the seasonal pycnocline. Near the shelfbreak (x = 75 km) the variance in temperature increases (note the deepening of the 2°C contour in the standard deviation field of Figure 6a); this is due to the intermittent presence of Bering summertime water (discussed in section 4). The predominant subsurface signal is the enhanced variability adjacent to the upper slope, between 100 and 200 m, in both temperature and salinity (and hence density). This is consistent with the fact that the cold signature of the winter-transformed Bering water, in the average temperature section of Figure 6a, weakens next to the slope. One might have expected a stronger mean signature of this water mass right at the boundary if it is being advected by a bathymetrically trapped current. Instead, the enhanced variability here keeps the mean winter water temperature more moderate. The nature of this subsurface variability is explored below.

3.2. Velocity

[20] In order to quantify the mean thermal wind signature described above (Figure 6c), we attempted to gather all the direct current meter measurements taken within the region of Figure 2. This proved to be difficult, however, since many of the historical data have fallen out of the public domain. Our only recourse was to compile the available published mean velocity records, of which we found 25. The sources of these values are listed in Table 2, and the locations of the instruments in the cross-stream plane are shown in Figure 4. A lateral plot of the mean vectors (Figure 8) reveals that the flow is generally to the east along the bathymetric contours (true for all but three of the vectors). We computed the component of flow along the local isobaths for each record, then projected these values onto the standard grid and applied the same interpolation scheme used above. Some additional Laplacian smoothing was done in order to filter out the few spurious points. Despite the fact that the measurement periods vary in length, season, and year, the resulting section of mean along-isobath flow (not shown) is contourable and well behaved. It shows a general increase in the eastwardly flow from about 50 m to 150 m.

[21] We used the interpolated field of current meter velocity to construct a mean vertical section of absolute geostrophic velocity. Specifically, the geostrophic transport per unit width was matched to the directly measured value (over the pertinent depth range) at each cross-stream location. The resulting absolute geostrophic velocity section is shown in Figure 9, and it reveals a feature that we call the Beaufort shelfbreak current, or jet. The jet is centered between 150 and 200 m depth (in the lower halocline), and is trapped against the continental slope. Its width is approximately 20 km, with a peak amplitude of $\sim$9 cm s^{-1}. Excluding the near-surface flow and the underlying Atlantic

Table 2. Mean Current Meter Velocities in the Study Region[a]

Mooring ID	Latitude (N)	Longitude (W)	Water Depth, m	Instrument Depth, m	Speed, cm s^{-1})	Direction, °T
OL	71°12.6′	149°53.0′	225	100	12.8	99
LO1	71°31.1′	152°11.3′	192	152	2.3	154
LO4	71°31.8′	152°15.3′	192	177	4.8	142
LO5	71°17.0′	150°44.1′	99	64	3.8	100
LO6	71°17.7′	150°37.9′	203	68	6.4	112
LO6	71°17.7′	150°37.9′	203	188	6.9	102
FLAX1	70°43.6′	146°0.0′	59	39	1.0	67
FLAX1	70°43.6′	146°0.0′	59	49	1.3	73
OL1	71°10.0′	148°52.7′	60	40	7.0	89
OL1	71°10.0′	148°52.7′	60	50	9.2	82
MB1	71°0.0′	146°45.8′	1008	83	1.5	168
MB1	71°0.0′	146°45.8′	1008	148	6.9	97
MB1	71°0.0′	146°45.8′	1008	980	0.0	0
MB2	70°55.1′	146°45.8′	170	62	0.3	181
MB2	70°55.1′	146°45.8′	170	95	5.0	112
MB2	70°55.1′	146°45.8′	170	145	8.0	103
MA2	71°41.5′	153°4.4′	162	60	3.5	291
MA2	71°41.5′	153°4.4′	162	93	0.1	219
MA2	71°41.5′	153°4.4′	162	143	7.8	119
MB2B	71°2.0′	146°45.8′	1022	72	5.9	113
MB2B	71°2.0′	146°45.8′	1022	105	7.6	110
MB2B	71°2.0′	146°45.8′	1022	155	6.6	109
MA2B	71°43.5′	153°4.4′	187	79	1.6	102
MA2B	71°43.5′	153°4.4′	187	112	3.3	130
MA2B	71°43.5′	153°4.4′	187	162	5.6	113

[a]These come from *Aagaard* [1984, 1989], *Aagaard and Roach* [1990], and K. Aagaard (personal communication, 2001).

water, the mean transport of the jet is 0.39 Sv. This is nearly half of the long-term mean volume flux through Bering Strait [*Roach et al.*, 1995], but at present it is unclear exactly what fraction of the jet is of Bering Strait origin (note also that the Bering Strait transport value is much more robust than the mean transport calculated here). Nonetheless, these results suggest that a sizable fraction of the Pacific water flowing into the Chukchi Sea eventually feeds a shelfbreak jet along the Alaskan Beaufort Sea (seasonally the transport is likely even larger, see section 4).

[22] The current structure revealed in Figure 9 should be thought of as a refinement to the concept of the ''Beaufort Undercurrent'' put forth by *Aagaard* [1984]. The earlier view was one of an eastward-flowing boundary current system that strengthened with depth down to the base of the continental slope. Our more robust analysis has demonstrated that there is instead a narrow, mid-depth intensified jet situated above the Atlantic layer (although, seasonally, some upwelled Atlantic water contributes to the flow as detailed below). Synoptically, the Beaufort shelfbreak jet can likely be significantly stronger, since some of the peak subtidal current meter speeds reported in the literature are >60 cm s^{-1} [e.g., *Aagaard*, 1984]. This, together with the vertical structure of the isopycnal tilt, suggests that the jet

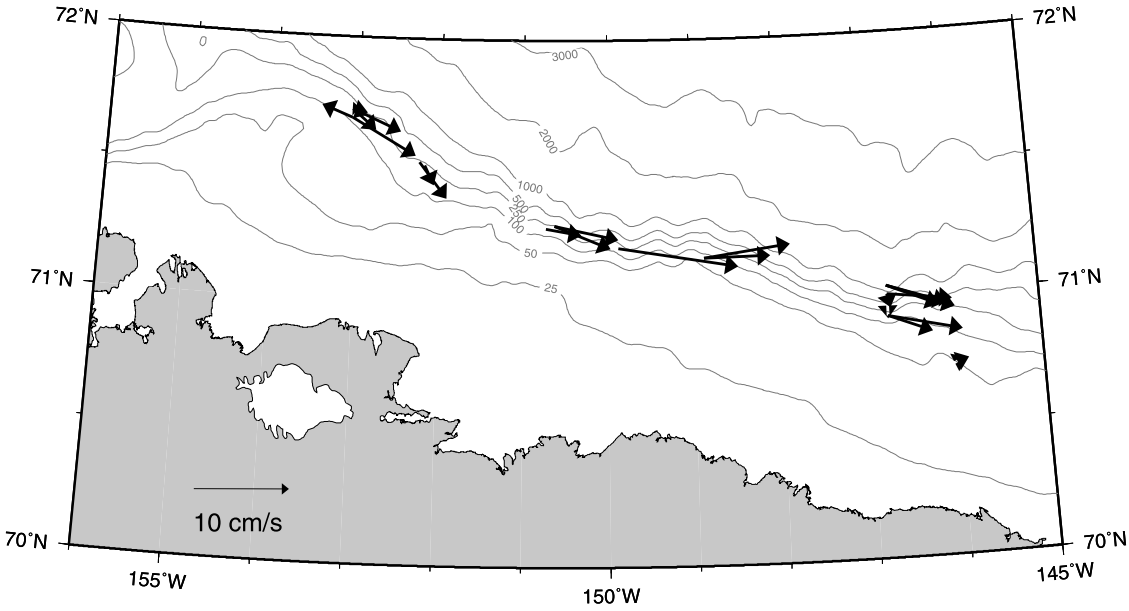

Figure 8. Mean current meter vectors within the study domain.

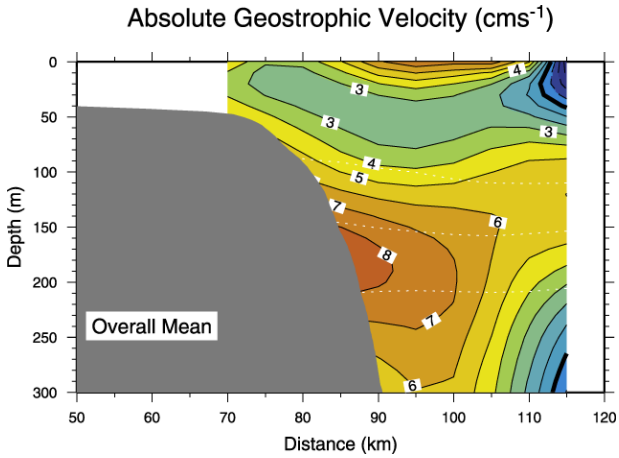

Figure 9. Mean absolute geostrophic velocity. The white dotted lines denote the upper and lower halocline.

may be hydrodynamically unstable. Note in Figure 6d that the cross-stream gradient in potential vorticity changes sign (e.g., it is negative at z = 90 m and positive at z = 130 m), thus satisfying the necessary condition for baroclinic instability. This lends support to the earlier hypothesis [e.g., *Manley and Hunkins*, 1985] that baroclinic instability of the shelf-edge flow along the Beaufort Sea may be partly responsible for the formation of eddies observed in the interior Canada Basin [e.g., *Plueddemann et al.*, 1999].

4. Seasonality

[23] The analysis of the average fields in the previous section presents several questions. For example, where is the so-called summertime Bering water? And why is the cold temperature core of winter-transformed Bering water not coincident (vertically or laterally) with the subsurface velocity core? The answers to these questions lie in the fact that the Beaufort shelfbreak jet is actually comprised of three distinct seasonal configurations.

4.1. Hydrography

[24] Inspection of the individual hydrographic sections reveals that the majority of sections can be classified into one of three separate categories. The first category is one in which there is a preponderance of summertime Bering water occupying the outer shelf and shelfbreak (we call this the summer water case). The second state is characterized by a strong presence of winter-transformed water (the winter water case), and the third state is one in which a substantial amount of Atlantic water resides at relatively shallow depths, banked up against the continental slope (the Atlantic water case). Altogether, seven sections correspond to the summer water case (from four different years), nine sections to the winter water case (four different years), and six sections to the Atlantic water case (three different years, see Table 1). Of the 11 remaining sections in our collection, six did not have the lateral coverage to make a determination, while the other five were ambiguous.

[25] To elucidate the three configurations of the jet, we computed the composite average hydrographic section for each case (Figure 10). In the summer water case (Figure 10a), one sees the warm, buoyant Bering summer water occupying the top 50 m, with the strongest temperature signal near the shelfbreak (approximately 3°C). Synoptically, this signal can be as warm as 5°C [see also *Mountain*, 1974]. The winter water composite (Figure 10b) shows a strong signature of winter-transformed Bering water (approximately −1.4°C) located against the upper continental slope. In both of these sections, there is a second, offshore enhancement of the temperature signal that appears somewhat detached from the boundary-trapped core (note the isolated warm core between 0 and 20 m near x = 105 km in Figure 10a, and the enhanced cold temperature between 110 and 150 m near x = 120 km in Figure 10b.) This is particularly evident in some of the individual sections, and a possible reason for it is discussed in section 6. Finally, the Atlantic water case (Figure 10c) contains water as warm as 0°C near 150 m depth, with a much stronger signature of Atlantic water against the slope.

[26] The immediate question is, do these configurations represent seasonal or interannual variability of the jet? Since each of the three states was present over multiple years, this

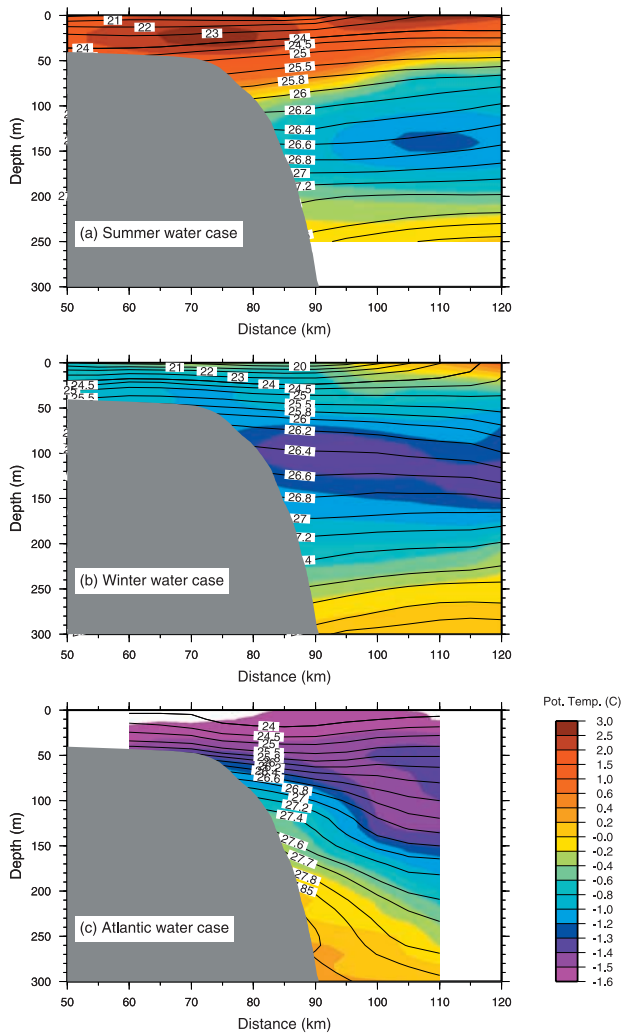

Figure 10. Seasonal composite hydrographic sections. Potential density (contours in kg m^{-3}) overlaid on potential temperature (color).

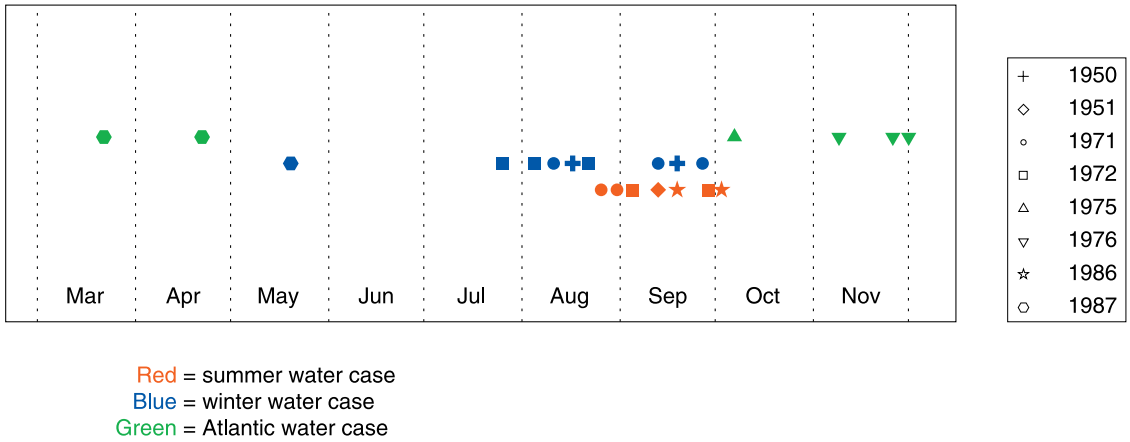

Figure 11. Seasonal distribution of sections used in the composite averages. Red symbols correspond to the summer water case, blue to the winter water case, and green to the Atlantic water case. The key to the right indicates the year of occupation.

suggests seasonality. To document this, we first made an advective correction to the time of occupation of each section, in an effort to account for the fact that the sections were occupied at different alongstream locations in the domain. Using an advective speed of 8 cm s^{-1} (suggested by Figure 9), we computed the yearday that each section would have been occupied had all of them been situated at a common location near the center of the domain. The adjustments ranged from 2 to 32 days, with a median of 13 days. The resulting seasonal distribution of sections is shown in Figure 11. While our total number of sections is relatively small, this distribution is nonetheless suggestive of a clear trend. Specifically, the winter water state (blue symbols) seems to be present from late spring through late summer, the summer water state (red symbols) from mid-summer through early fall, and the Atlantic water state (green symbols) from mid-fall through mid-spring.

[27] This seasonal transition of the Beaufort shelfbreak jet becomes even more meaningful when one considers the timing of the wind and buoyancy forcing in the region. As detailed by *Weingartner et al.* [1998], during the time of winter transformation in the northeast Chukchi Sea, the winds can retard (or possibly block) the northward flow of Pacific water toward the Beaufort Sea. After the winter winds subside, the dense water on the Chukchi shelf is likely flushed out more readily; this is consistent with the timing of the winter-transformed signal seen in the Beaufort shelfbreak jet (Figure 11). With the advent of spring, the warm water flowing through Bering Strait once again establishes the Alaskan coastal current flowing along the eastern Chukchi Sea [*Roach et al.*, 1995]. This water is believed to take approximately 2 months to reach Barrow Canyon [*Mountain*, 1974; *Weingartner et al.*, 1998], which means it would appear in the Alaskan Beaufort Sea in mid-to-late summer, again consistent with Figure 11 [see also *Mountain*, 1974].

[28] The appearance of the summertime Bering water in our sections also coincides with the period of reversed summertime winds in the Beaufort Sea. Over most of the year the winds in this region are easterly (part of the large-scale anti-cyclonic wind system that drives the interior Beaufort Gyre). However, during August and September the winds reverse locally and are generally out of the west [*Furey*, 1996]. This would tend to reinforce the eastward flow of near-surface summertime Bering water in the Beaufort shelfbreak jet. Later in the fall (and winter) the winds are easterly once more and therefore are upwelling favorable along the Alaskan northern slope. Hence one might expect to see Atlantic water at shallower depths against the continental slope, as is observed during the fall/winter time period (Figures 10c and 11). Therefore the three configurations of the Beaufort shelfbreak jet, as well as their relative timing over the course of the year, are consistent with the different water mass sources and regional atmospheric forcing.

[29] In Figure 11 it is seen that there is some overlap between the seasonal configurations of the jet. Indeed, the summer water composite section (Figure 10a) contains a core of winter-transformed water at depth (albeit weaker than in the winter water composite). Sometimes, sections from the same cruise can contain realizations that fall into two different categories. This is not surprising since the seasonal transitions in the forcing discussed above are not abrupt. For example, a recent hydrographic section taken across the mouth of Barrow Canyon in August 2002 (at the western edge of our domain) revealed simultaneous advection of both summertime Bering water and winter-transformed Bering water toward the Beaufort Sea [*Pickart and Weingartner*, 2003].

4.2. Velocity

[30] The density structure of the three seasonal composites of the Beaufort shelfbreak jet (Figure 10) indicate that the flow structure of the jet is substantially different in each case. To quantify this, we computed the thermal wind shear and corresponding relative geostrophic velocity section for each case. Note in Figure 10a that in the summertime configuration the isopycnals slope downward near the boundary, especially in the vicinity of the shelfbreak. This is reminiscent of typical surface-intensified shelfbreak jets found at midlatitudes, for example the Labrador Current [*Lazier and Wright*, 1993] and the Middle Atlantic Bight shelfbreak jet [*Linder and Gawarkiewicz*, 1998]. Since only mean current meter values were available, we were unable

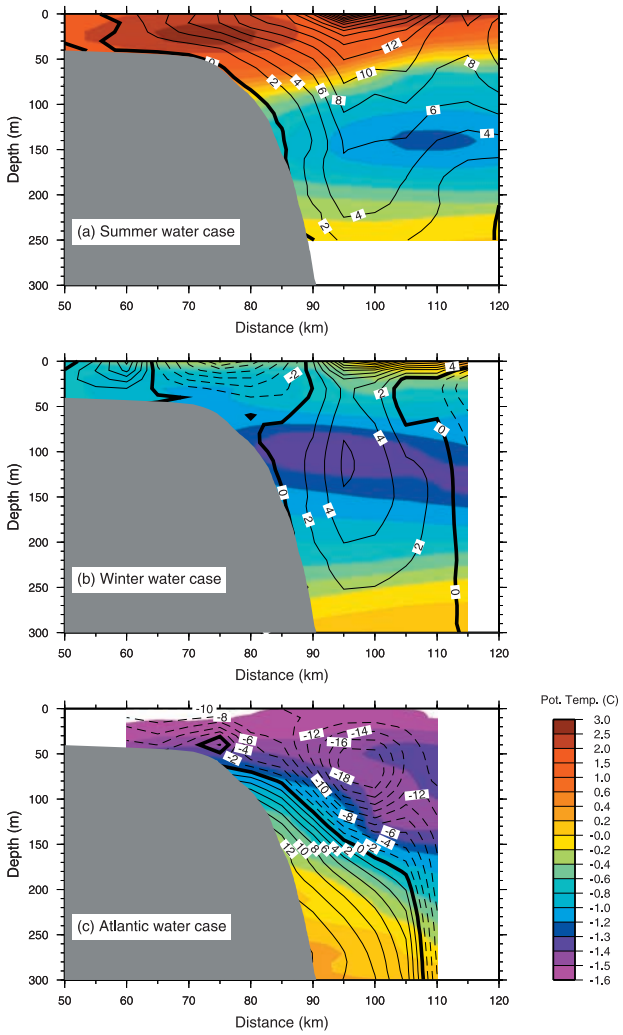

Figure 12. Seasonal composite geostrophic velocity sections (contours in cm s^{-1}) overlaid on potential temperature (color). The choice of reference velocity for each case is discussed in the text.

to do a seasonal referencing of the jet. Hence we had to make subjective choices regarding a level of known motion. For the summertime composite, the near-surface warm layer is clearly flowing eastward at a faster rate than the water at depth; therefore we chose 350 m as a depth of no motion (for water depths shallower than this the bottom was taken to be the level of no motion).

[31] The resulting geostrophic velocity section (Figure 12a) reveals a relatively swift jet advecting the summertime Bering water toward the Canadian Beaufort Sea. The transport of the jet (excluding the Atlantic water) is 0.64 Sv. Since our reference level of no motion is within the Atlantic layer, which is likely flowing eastward itself at this time of year, this transport estimate is probably too small. Furthermore, the flow at the bottom is likely non-zero, as is the case for the midlatitude jets mentioned above. This suggests that during certain times of the year, the Beaufort shelfbreak jet can transport as much water as is flowing through Bering Strait. We note that if there is flow along the bottom (i.e., a significant barotropic component), this would change the structure of the jet somewhat from that depicted in Figure 12a. For example, one could easily imagine stronger flow at the shelfbreak, coincident with the warm core of the Bering summer Water.

[32] For the winter water case the isopycnal tilt is more reminiscent of the mean section: upward sloping density contours toward the shallow part of the slope, and downward sloping contours at deeper depths. Using the same choice for a reference level as above (with the same caveats), one sees that this configuration corresponds to a mid-depth jet, centered at the depth of the winter-transformed Bering water (approximately 100 m, Figure 12b) (the flow in the shallow layer (upper 30 m), across the length of the section, is not considered in this discussion). This makes perfect sense: The strongest eastward flow is that of the dense water being flushed out of the Chukchi Sea. We note again that a barotropic component likely exists, which would increase the amplitude of the jet adjacent to the slope. This means that the jet would remain strong at 100 m as one approaches the boundary (instead of decreasing to zero as it does in Figure 12b), or perhaps even increase shoreward in the sense of a boundary-trapped jet, as in the mean section.

[33] The Atlantic water case has yet a third flow structure. The density section (Figure 10c) is dominated by a strong upward tilt of the isopycnals at mid-depth. As discussed above, this case is found in the fall to spring upwelling season, so the near-surface water is likely flowing to the west as a result of wind set up. At some deeper level, however, the Atlantic water is still flowing eastward, which means there is a flow reversal at some unknown depth. Hence, instead of specifying a priori the level of no motion, it is of interest to determine where this reversal occurs using a more objective approach. As noted earlier, the historical current meter time series data are unaccessible; however, there have been a few recent moored measurements along the Beaufort slope which suggest that the flow above the main pycnocline during winter is on the order of 10 cm s^{-1} to the west (K. Shimada, personal communication, 2003). Consequently, we referenced the Atlantic water case by specifying a surface velocity of this magnitude everywhere across the section. Admittedly, this is not precise, but the resulting geostrophic velocity section is quite reasonable (Figure 12c): The level of no motion roughly parallels the isopycnals near the slope, indicating that all of the Atlantic water, as well as some of the colder water above it, is flowing eastward, beneath the wind-driven surface layer.

[34] Returning now to the average configuration of the Beaufort shelfbreak jet (Figures 6 and 9), it is clear that the presence of summertime Bering water is so short-lived (mid-summer to early fall) that it does not influence the overall mean. Furthermore, the seasonal composite sections solve the quandary regarding the non-coincidence of the mean velocity core and cold temperature core. The presence of both the warm Bering water, as well as upwelled Atlantic water, keep the mean temperatures more moderate next to the upper slope (and lead to the enhanced temperature standard deviation there, Figure 6a). At the same time the differing seasonal isopycnal slopes combine to produce a deeper mean velocity core. The winter water composite does reveal, however, that during the time of year when the

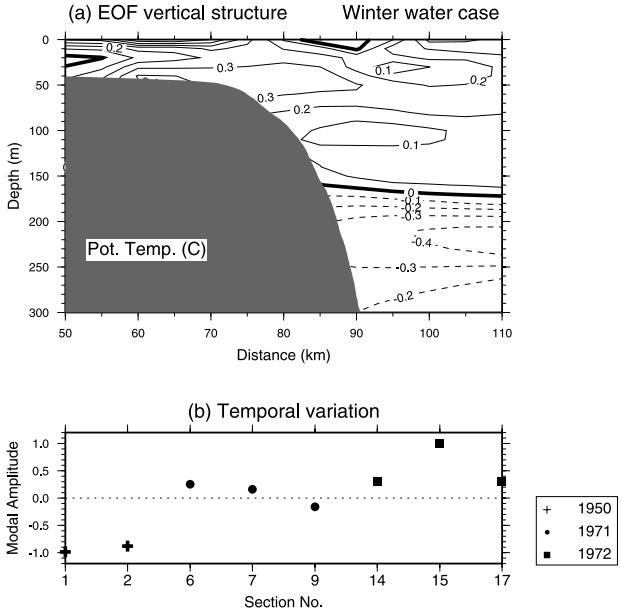

Figure 13. Dominant coupled temperature/density EOF mode for the winter water sections. (a) Vertical structure of temperature; (b) Modal amplitude time series. Multiplying values from Figures 13a and 13b together gives the dimensional value of the mode. (Note that the vertical structure represents the maximum dimensional value of the mode in °C.)

dense water from the Chukchi Sea is found along the Beaufort slope, the velocity and temperature cores do indeed coincide.

5. Interannual Variability

[35] To investigate the longer timescale variability of the Beaufort shelfbreak jet, we performed an empirical orthogonal function (EOF) analysis on the collection of sections representing the winter water case. (The single springtime occupation in this collection was omitted in order to minimize any seasonal aliasing.) The reader is referred to *Pickart et al.* [1999] for a discussion of the methodology. Separate calculations were done on the temperature, salinity, and density sections alone, as well as a coupled temperature/density calculation. Despite the relatively small number of realizations, a consistent dominant mode emerged in each case. We present results from the coupled temperature/density calculation, in which the first mode explains 47% of the variance (more than twice that of the next mode).

[36] The vertical structure of the dominant mode (Figure 13a) shows that the upper 150 m of the water column is out of phase with the deeper water. In other words, warming at shallower depths is associated with cooling at deeper depths (and vice versa). To get a better idea of what this means in terms of the winter-transformed Bering water signal, we added ±1 standard deviation of the modal amplitude back into the mean, and the resulting sections are shown in Figure 14. The two states can be summarized as follows. In the first configuration (Figure 14a) the winter water temperature signal is colder, but it is confined to a lighter, more stratified density layer (25.8–26.9 kg m^{-3}). In the second configuration (Figure 14b) the temperature signal is weaker, but it is spread out over more of the water column within a heavier, more uniform density layer (26.2–27.1 kg m^{-3}). In both cases the thermal wind shear is oppositely signed above and below the winter-transformed water (as was the case for the seasonal composite, Figure 10b), indicating the presence of the Beaufort shelfbreak jet. The time series of modal amplitudes (Figure 13b) shows that the winter water was at its cold extreme in 1950, and at its warm extreme in 1972.

[37] As mentioned earlier, on average the winter-transformed Bering water is ventilating the upper halocline. Although our sample size is small, the EOF results suggest that this is true as well from year to year. Even in the dense case the young Pacific-origin water occupies predominantly the upper halocline; in the other modal extreme it is found at depths above the upper halocline as well. Does the variability captured by the EOF make sense in terms of the formation of the winter-transformed Bering water in the Chukchi Sea? While one might anticipate that a colder signal means a denser product, Figure 14 indicates that this is not the case. This is consistent with the idea that the winter water is always formed at or near the freezing point (i.e., there is little variation in source temperature). The EOF also suggests that a denser product is associated with less stratification. This is reasonable in that more rigorous convection on the Chukchi shelf should result in a more uniform water mass. The only curious aspect of the EOF is that denser winter water is apparently warmer. Such a scenario may be associated with stronger outflow from the Chukchi, which is likely to result in a more unstable

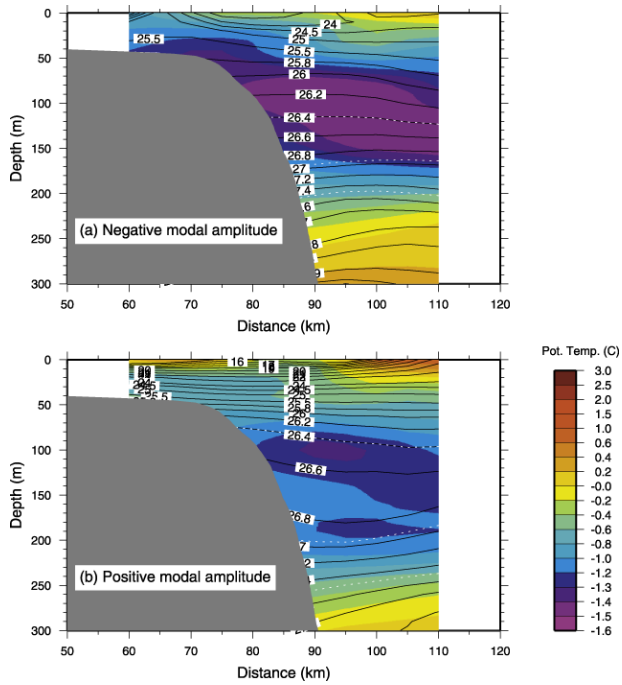

Figure 14. A 1-standard-deviation negative and positive modal amplitude added back into the mean field. Potential density is contoured (kg m^{-3}), and potential temperature is colored. The white dotted lines denote the upper and lower halocline.

Beaufort shelfbreak jet. This would cause more turbulent exchange with the surrounding water, for example, through eddy formation, and in turn modify the temperature (and silicate) signal more extensively.

6. Discussion

[38] The results presented above have demonstrated the existence of the Beaufort shelfbreak jet, which presumably carries much of the outflowing water from the Chukchi Sea toward the eastern Canada Basin. The jet is comprised of three seasonally distinct states, associated with the advection of summertime Bering water, winter-transformed Bering water, and upwelled Atlantic water. Despite our detailed analysis, the volume transport of the jet, and especially the seasonal modulation in transport, cannot be quantitatively established from the historical data. In light of the complex seasonal modification of Pacific-origin waters in the Chukchi Sea [*Weingartner et al.*, 1998], as well as the strong interannual variability in the circulation of the sea [e.g., *Woodgate et al.*, 2003], quantifying the volume flux will not be a trivial matter. A network of moorings has recently been deployed as part of the Western Arctic Shelf-Basin Interactions Program (SBI) to measure the different Chukchi outflow points simultaneously with the flow along the Beaufort shelfbreak. It is hoped this will elucidate the transport pathways and seasonality of the Chukchi/Beaufort boundary current system.

[39] As mentioned earlier, the structure of the Beaufort shelfbreak jet is conducive for baroclinic instability. In particular, the mid-depth intensified winter water state satisfies the necessary condition for baroclinic instability, and the surface-intensified flow of the summer state is analogous to the Middle Atlantic Bight shelfbreak jet, which is highly unstable [e.g., *Garvine et al.*, 1988; *Fratantoni and Pickart*, 2003]. Some of the synoptic geostrophic velocity sections from *Mountain* [1974], corresponding to the summer water state, also reveal very strong lateral velocity shears, on the order of the local Coriolis parameter. *Paquette and Bourke* [1974] reported instantaneous current speeds of 100 cm s^{-1} in this region, consistent with such shears. This suggests that barotropic instability may be active at times as well [see also *Manley and Hunkins*, 1985].

[40] It has been argued that hydrodynamic instability of the boundary current along the Beaufort slope is in fact responsible for some of the small-scale eddies observed in the interior of the Canada Basin [*Hunkins*, 1974; *Manley and Hunkins*, 1985]. The western Arctic seems to be full of such eddies, which are predominantly subsurface anticyclones [*Manley and Hunkins*, 1985]. Recently, *Muench et al.* [2000] did a detailed analysis of an anti-cyclonic eddy observed to the north of our study area and found that the water within the core was of Pacific origin, including a high concentration of silicate. A detailed census of the eddies observed during the AIDJEX and IOEB observational programs, covering seven different years, indicates that the majority of eddy centers are situated between 50 and 150 m [*Manley and Hunkins*, 1985; *Krishfield and Plueddemann*, 2002], with core temperatures predominantly between −1.7 and −1.2°C (A. Plueddemann, personal communication, 2003). By comparison, the minimum and maximum temperatures of the winter-transformed water in our coupled EOF are −1.5 and −1.3°C, respectively (keep in mind, however, that the EOF contains data from only 3 years).

[41] *Shaw and Chao* [2003] purport that subsurface eddies are formed from the outflowing dense water through Barrow Canyon, and the model density field in their Figure 5a exhibits a structure reminiscent of our mean density field (Figure 6c). However, the mechanism studied by *Shaw and Chao* [2003] relies strongly on the presence of the canyon, as well as the westward-flowing Beaufort Gyre. In a follow up study, *Chao and Shaw* [2003] argue that the Beaufort Undercurrent, as envisaged by *Aagaard* [1984], also plays an important role in the spawning of such eddies. Our results seem to contradict these conclusions, since there is no evidence of the Beaufort Gyre or a deep-reaching undercurrent adjacent to the Beaufort shelfbreak. *Manley and Hunkins* [1985] suggest that the summertime Bering water may be the origin of some of the warm core eddies observed offshore.

[42] Although our study has focused on seasonal to interannual timescales, it is worth noting that certain features in our sections are consistent with the notion of local mesoscale eddy formation to the east of Barrow Canyon. For example, the standard deviation of temperature shows an offshore enhancement of variance, near the edge of the section, both near the surface and near the depth of the upper halocline, i.e., close to the core depths of the summer and winter-transformed Bering water (Figure 6a). The composite mean sections of Figures 10a and 10b also give the impression of offshore pinching of these water mass cores. While this is only anecdotal evidence, when considered together with the above discussion regarding hydrodynamic instability, it suggests that the Beaufort shelfbreak jet may be an important source of the eddies observed in the western Arctic. Ongoing work within the SBI program is directed at testing this hypothesis.

[43] **Acknowledgments.** The author is indebted to Knut Aagaard, who provided some of the current meter and nutrient data, and was involved in many of the field programs that produced the hydrographic sections. His insights and advice were a great help in interpreting the results. Terry McKee helped with numerous aspects of the data analysis, and Roger Goldsmith assisted with the calculations using the IBCAO data. This work was supported by the Office of Naval Research under contract N00014-98-1-0046. WHOI contribution number 10910.

References

Aagaard, K. (1984), The Beaufort Undercurrent, in *The Alaskan Beaufort Sea: Ecosystems and Environments*, pp. 47–71, Academic, San Diego, Calif.

Aagaard, K. (1989), A synthesis of the Arctic Ocean circulation, *Rapp. P. V. Reun. Cons. Int. Explor. Mer.*, *188*, 11–22.

Aagaard, K., and A. T. Roach (1990), Arctic ocean-shelf exchange: Measurements in Barrow Canyon, *J. Geophys. Res.*, *95*, 18,163–18,175.

Aagaard, K., L. K. Coachman, and E. C. Carmack (1981), On the halocline of the Arctic Ocean, *Deep Sea Res.*, *28*, 529–545.

Cavalieri, D. J., and S. Martin (1994), The contribution of Alaskan, Siberian, and Canadian coastal polynyas to the cold halocline layer of the Arctic Ocean, *J. Geophys. Res.*, *99*, 18,343–18,362.

Chao, S.-Y., and P.-T. Shaw (2003), Heton shedding from submarine-canyon plumes in an Arctic boundary current system: Sensitivity to the undercurrent, *J. Phys. Oceanogr.*, *33*, 2032–2044.

Chapman, D. C. (2000), The influence of an alongshelf current on the formation and offshore transport of dense water from a coastal polynya, *J. Geophys. Res.*, *105*, 24,007–24,019.

Fratantoni, P. S., and R. S. Pickart (2003), Variability of the shelfbreak jet in the Middle Atlantic Bight: Internally or externally forced?, *J. Geophys. Res.*, *108*, 3166, doi:10.1029/2002JC001326.

Furey, P. W. (1996), The large-scale surface wind field over the western Arctic ocean, 1981–1993, Masters thesis, 121 pp., Univ. of Alaska, Fairbanks.
Garrison, G. R., and P. Becker (1976), The Barrow submarine canyon: A drain for the Chukchi Sea, *J. Geophys. Res.*, *81*, 4445–4453.
Garvine, R. W., K. C. Wong, G. G. Gawarkiewicz, R. K. McCarthy, R. W. Houghton, and F. Aikman III (1988), The morphology of shelfbreak eddies, *J. Geophys. Res.*, *93*, 15,593–15,607.
Gawarkiewicz, G. G. (2000), Effects of ambient stratification and shelfbreak topography on offshore transport of dense water on continental shelves, *J. Geophys. Res.*, *105*, 3307–3324.
Hunkins, K. L. (1974), Subsurface eddies in the Arctic Ocean, *Deep Sea Res.*, *21*, 1017–1033.
Jones, E. P., and L. G. Anderson (1986), On the origin of the chemical properties of the Arctic Ocean halocline, *J. Geophys. Res.*, *91*, 10,759–10,767.
Krishfield, R. A., and A. J. Plueddemann (2002), Eddys in the Arctic Ocean from IOEB ADCP data, *Tech. Rep. WHOI-2002-09*, 144 pp., Woods Hole Oceanogr. Inst., Woods Hole, Mass.
Lazier, J. R. N., and D. G. Wright (1993), Annual velocity variations in the Labrador Current, *J. Phys. Oceanogr.*, *23*, 559–678.
Linder, C. A., and G. G. Gawarkiewicz (1998), A climatology of the shelfbreak front in the Middle Atlantic Bight, *J. Geophys. Res.*, *103*, 18,405–18,423.
Manley, T. O., and K. Hunkins (1985), Mesoscale eddies of the Arctic Ocean, *J. Geophys. Res.*, *90*, 4911–4930.
Melling, H. (1998), Hydrographic changes in the Canada basin of the Arctic Ocean, 1979–1996, *J. Geophys. Res.*, *103*, 7637–7645.
Mountain, D. G. (1974), Bering Sea Water on the north Alaskan shelf, Ph.D. thesis, 153 pp., Univ. of Wash., Seattle.
Muench, R. D., J. D. Schumacher, and S. A. Salo (1988), Winter currents and hydrographic conditions on the northern central Bering Sea shelf, *J. Geophys. Res.*, *93*, 516–526.
Muench, R. D., J. T. Gunn, T. E. Whitledge, P. Schlosser, and W. Smethie Jr. (2000), An Arctic Ocean cold core eddy, *J. Geophys. Res.*, *105*, 23,997–24,006.
Munchow, A., and E. C. Carmack (1997), Synoptic flow and density observations near an Arctic shelfbreak, *J. Phys. Oceanogr.*, *27*, 1402–1419.
Paquette, R. G., and R. H. Bourke (1974), Observations on the coastal current of Arctic Alaska, *J. Mar. Res.*, *32*, 195–207.
Pickart, R. S. (1992), Space-time variability of the deep western boundary current oxygen core, *J. Phys. Oceanogr.*, *22*, 1047–1061.
Pickart, R. S., and T. J. Weingartner (2003), Shelfbreak circulation in the Alaskan Beaufort Sea, paper presented at Western Arctic Shelf-Basin Interactions (SBI) Principle Investigators Meeting, Natl. Sci. Found., Miami, Fla.
Pickart, R. S., T. K. McKee, D. J. Torres, and S. A. Harrington (1999), Mean structure and interannual variability of the slopewater system south of Newfoundland, *J. Phys. Oceanogr.*, *29*, 2541–2558.
Plueddemann, A., R. Krishfield, and C. Edwards (1999), Eddies in the Beaufort Gyre, paper presented at Ocean-Atmosphere-Ice Interactions (OAII) All Hands Meeting, Natl. Sci. Found., Virginia Beach, Va.
Roach, A. T., A. Aagaard, C. H. Pease, S. A. Salo, T. Weingartner, V. Pavlov, and M. Kulakov (1995), Direct measurements of transport and water properties through the Bering Strait, *J. Geophys. Res.*, *100*, 18,443–18,457.
Rudels, B., E. P. Jones, L. G. Anderson, and G. Kattner (1994), On the intermediate depth waters of the Arctic Ocean, in *The Polar Oceans and Their Role in Shaping the Global Environment*, *Geophys. Monogr. Ser.*, vol. 85, edited by O. M. Johannessen et al., pp. 33–46, AGU, Washington, D. C.
Shaw, P.-T., and S.-Y. Chao (2003), Effects of a baroclinic current on a sinking dense water plume from a submarine canyon and heton shedding, *Deep Sea Res., Part I*, *50*, 357–370.
Shimada, K., E. C. Carmack, K. Hatakeyama, and T. Takizawa (2001), Varieties of shallow temperature maximum waters in the western Canadian basin of the Arctic Ocean, *Geophys. Res. Lett.*, *28*, 3441–3444.
Smith, J. N., S. B. Moran, and R. W. Macdonald (2003), Shelf-basin interactions in the Arctic Ocean base on ^{2}10Pb and Ra isotope tracer distributions, *Deep Sea Res., Part I*, *50*, 397–416.
Weingartner, T. J., D. J. Cavalieri, K. Aagaard, and Y. Sasaki (1998), Circulation, dense water formation, and outflow on the northeast Chukchi shelf, *J. Geophys. Res.*, *103*, 7647–7661.
Winsor, P., and D. C. Chapman (2002), Distribution and interannual variability of dense water production from coastal polynyas on the Chukchi shelf, *J. Geophys. Res.*, *107*(C7), 3079, doi:10.1029/2001JC000984.
Woodgate, R. A., K. Aagaard, T. J. Weingartner (2003), A year in the physical oceanography of the Chukchi Sea 1990–1991, paper presented at Western Arctic Shelf-Basin Interactions (SBI) Principle Investigators Meeting, Natl. Sci. Found, Miami, Fla.

R. S. Pickart, Department of Physical Oceanography, Woods Hole Oceanographic Institution, MS 21, Woods Hole, MA 02543, USA. (rpickart@whoi.edu)